Journal of Applied Physics

Robust high pressure stability and negative thermal expansion in sodium-rich antiperovskites Na_3OBr and Na_4OI_2

Cite as: J. Appl. Phys. **119**, 025901 (2016); https://doi.org/10.1063/1.4940020
Submitted: 22 October 2015 . Accepted: 05 January 2016 . Published Online: 14 January 2016

Yonggang Wang, Ting Wen, Changyong Park, Curtis Kenney-Benson, Michael Pravica, Wenge Yang, and Yusheng Zhao

Robust high pressure stability and negative thermal expansion in sodium-rich antiperovskites Na_3OBr and Na_4OI_2

Yonggang Wang,[1,2,3,a)] Ting Wen,[2] Changyong Park,[4] Curtis Kenney-Benson,[4] Michael Pravica,[1] Wenge Yang,[3,5,a)] and Yusheng Zhao[1,a)]
[1]*High Pressure Science and Engineering Center, University of Nevada, Las Vegas, Nevada 89154, USA*
[2]*Institute of Nanostructured Functional Materials, Huanghe Science and Technology College, Zhengzhou, Henan 450006, China*
[3]*High Pressure Synergetic Consortium (HPSynC), Geophysical Laboratory, Carnegie Institution of Washington, Argonne, Illinois 60439, USA*
[4]*High Pressure Collaborative Access Team (HPCAT), Geophysical Laboratory, Carnegie Institution of Washington, Argonne, Illinois 60439, USA*
[5]*Center for High Pressure Science and Technology Advanced Research (HPSTAR), Shanghai 201203, China*

(Received 22 October 2015; accepted 5 January 2016; published online 14 January 2016)

The structure stability under high pressure and thermal expansion behavior of Na_3OBr and Na_4OI_2, two prototypes of alkali-metal-rich antiperovskites, were investigated by *in situ* synchrotron X-ray diffraction techniques under high pressure and low temperature. Both are soft materials with bulk modulus of 58.6 GPa and 52.0 GPa for Na_3OBr and Na_4OI_2, respectively. The cubic Na_3OBr structure and tetragonal Na_4OI_2 with intergrowth K_2NiF_4 structure are stable under high pressure up to 23 GPa. Although being a characteristic layered structure, Na_4OI_2 exhibits nearly isotropic compressibility. Negative thermal expansion was observed at low temperature range (20–80 K) in both transition-metal-free antiperovskites for the first time. The robust high pressure structure stability was examined and confirmed by first-principles calculations among various possible polymorphisms qualitatively. The results provide in-depth understanding of the negative thermal expansion and robust crystal structure stability of these antiperovskite systems and their potential applications.
 [http://dx.doi.org/10.1063/1.4940020]

I. INTRODUCTION

Over the past decades, perovskite materials have been extensively studied owing to their significant properties such as ferroelectricity, exotic magnetism, superconductivity, and colossal magnetoresistance. Despite of their seemingly simple structure, the archetypal perovskite has a general formula ABO_3 with a large built-in potential for complex and desirable structure design.[1,2] Therefore, multitudinous functionalities have been demonstrated in perovskite-type materials by elemental doping, non-stoichiometries, intergrowth layer construction, and subtle BO_6 octahedra tilting/distortions. In contrast, as an emerging functional family with similar structure features, antiperovskite-type materials have attracted less attention.[3,4] Generally, antiperovskites are inorganic compounds with a perovskite structure but electronically inverted (e.g., $A^{m-}B^{(3n-m)-}X^{n+}{}_3$). The ideal antiperovskite structure adopts cubic $Pm\text{-}3m$ symmetry and also possesses the structural flexibility and built-in capabilities to form a complex structure comparable to those of the traditional perovskites. The other important feature of antiperovskite structure is the "X^{n+}-rich" composition. For example, in Mn_3AB (A = C, N, P, As; B = Mg, In, Ga, Al), the magnetic cations are located at the vertices of BMn_6 octahedron with strong interactions, which result in some interesting phenomenon such as magnetism involved negative thermal expansion (NTE).[5–10] In other examples, high ionic conductivities have been observed within alkali-metal-rich Li_3OX and Na_3OX owing to the convenient ionic migration along the edge of OLi_6 or ONa_6 octahedra.[11–14]

There are a very limited number of materials displaying "abnormal" NTE, which is against the "expansion and contraction law" in nature. It is expected that these materials will fall in various applications via controlled thermal expansion composites. Current research efforts mainly focus on the structure mechanism and extension of NTE over a large temperature range.[15–17] Examples of the most studied NTE materials include ZrW_2O_8,[18–20] metal-organic frameworks $Ag_3[Co(CN)_6]$,[21] and ReO_3-type compounds such as ScF_3.[22,23] Beyond this, NTE has also been observed in antiperovskite materials. Pure and elemental doped Mn_3AN (A = Zn, Ga, Cu) compounds were reported to exhibit giant negative thermal expansion.[24–27] Moreover, adjustable and zero thermal expansion can be achieved by modulating the Mn occupancy in $Mn_3Cu_{0.5}Ge_{0.5}N$ antiperovskite.[28] However, so far the NTE phenomenon has only been reported in transition metal dominated antiperovskites. NTE in lattice-only antiperovskite, similar as that of the ReO_3-type structure within perovskite family, has never been observed until now.

Alkali-metal-rich Na_3OBr and Na_4OI_2 present two archetypes of cubic and layered intergrowth antiperovskite structures and have been proposed as sources of solid-state sodium ionic electrolytes recently.[14] Fig. 1 shows the crystal structures of perovskite $CaTiO_3$, antiperovskites Na_3OBr and Na_4OI_2 for comparison. The crystal structure of conventional

a)Electronic addresses: yyggwang@gmail.com; yangwg@hpstar.ac.cn; and yusheng.zhao@unlv.edu

perovskite comprises corner-sharing BO_6 octahedra (e.g., TiO_6 in $CaTiO_3$ in Fig. 1(a)), where the O^{2-} anions serve as ligands. In contrast, antiperovskite Na_3OBr crystallizes in a cubic structure under normal conditions, where *A* and *B* sites are occupied by inversely charged Br^- and O^{2-}, and Na^+ cations serve as ligands (Fig. 1(b)). Na_4OI_2 presents an intergrowth of antiperovskite "Na_3OI" layers and NaI rock-salt layers, similar to the K_2NiF_4-type structure in perovskite (Fig. 1(c)). From the viewpoint of structural chemistry, distinct compressibility and thermal expansion behavior (isotropic and anisotropic) and also routine symmetry breaking under high pressure are expected in these materials.

In this paper, we employ study the compressibility and thermal expansion behavior of transition-metal-free antiperovskites Na_3OBr and Na_4OI_2. One of our aims is to investigate the structural variability of alkali-metal-rich antiperovskite under high pressure and low temperature conditions. And also, we try to obtain an in-depth understanding of the stability of antiperovskite based on the inversely charged-octahedra frameworks.

II. EXPERIMENTAL

Na_3OBr and Na_4OI_2 powders were synthesized via a solid state method starting from Na, NaOH, NaBr, and NaI.[14] After confirming the phase purity by routine X-ray diffraction (XRD) measurements, the materials were ground and loaded into a symmetrical diamond anvil cell (DAC) under Ar gas for high pressure studies. The *in situ* high pressure angle-dispersive XRD experiments were carried out at 16 BM-D station[29] of High-Pressure Collaborative Access Team (HPCAT) at the Advanced Phonon Source (APS), Argonne National Laboratory (ANL). A focused monochromatic X-ray beam with about 5 μm in diameter (FWHM) and wavelengths of 0.4246 Å was used for the diffraction experiments. *In situ* temperature-dependent XRD experiments from room temperature to 10 K were performed at the same beamline and with the samples from the same batch used in the *in situ* high pressure studies.

The total energy as functions of pressure, cell volume, and distortion degrees were calculated using the plane-wave pseudopotential method based on density functional theory with CASTEP package.[30] The exchange-correlation functional is described by the local density approximation (LDA).[31] The refined cubic crystal structure of Na_3OBr from our previous study[14] was adopted as the starting structure model, and the distorted structures in tetragonal and trigonal symmetries were generated artificially.

III. RESULTS AND DISCUSSION

A. Phase stability of Na_3OBr and Na_4OI_2 under pressure

Fig. 2 shows the *in situ* synchrotron XRD pattern of Na_3OBr and Na_4OI_2 under compression and decompression at room temperature, respectively. The cubic antiperovskite structure of Na_3OBr is stable up to 24.3 GPa, and all XRD patterns can be well indexed in the *Pm*-3*m* space group. After decompression, the sample return to a similar cell volume observed at ambient conditions. It is surprise that there is no phase transition to lower symmetry, for example, tetragonal or trigonal phase, has been observed for such a simple cubic antiperovskite subjected to high pressure. On the other hand, for Na_4OI_2, the tetragonal structure is maintained up to 24.3 GPa upon compression, despite we observed the broadening of XRD peaks, which are due to strains and partial amorphization. The decompression-recovered XRD pattern of Na_4OI_2 can be well indexed in space group *I*4/*mmm*, and the difference of some peak intensities with respect to that of the pristine pattern may be due to orientational preferences under pressure. The absence of symmetry breakdown in both Na_3OBr and Na_4OI_2 under pressure is interpreted due to the pseudo-rigid building block of ONa_6 octahedron, which will be further discussed in the following theoretical calculation section.

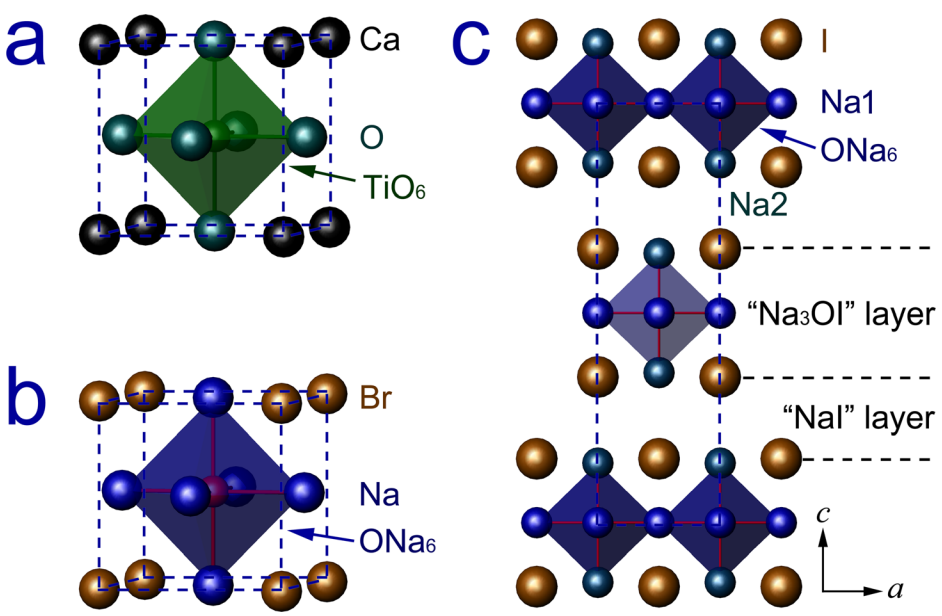

FIG. 1. Crystal structures of (a) cubic perovskite $CaTiO_3$, (b) cubic antiperovskite Na_3OBr, and (c) layered Na_4OI_2 with an intergrowth antiperovskite structure.

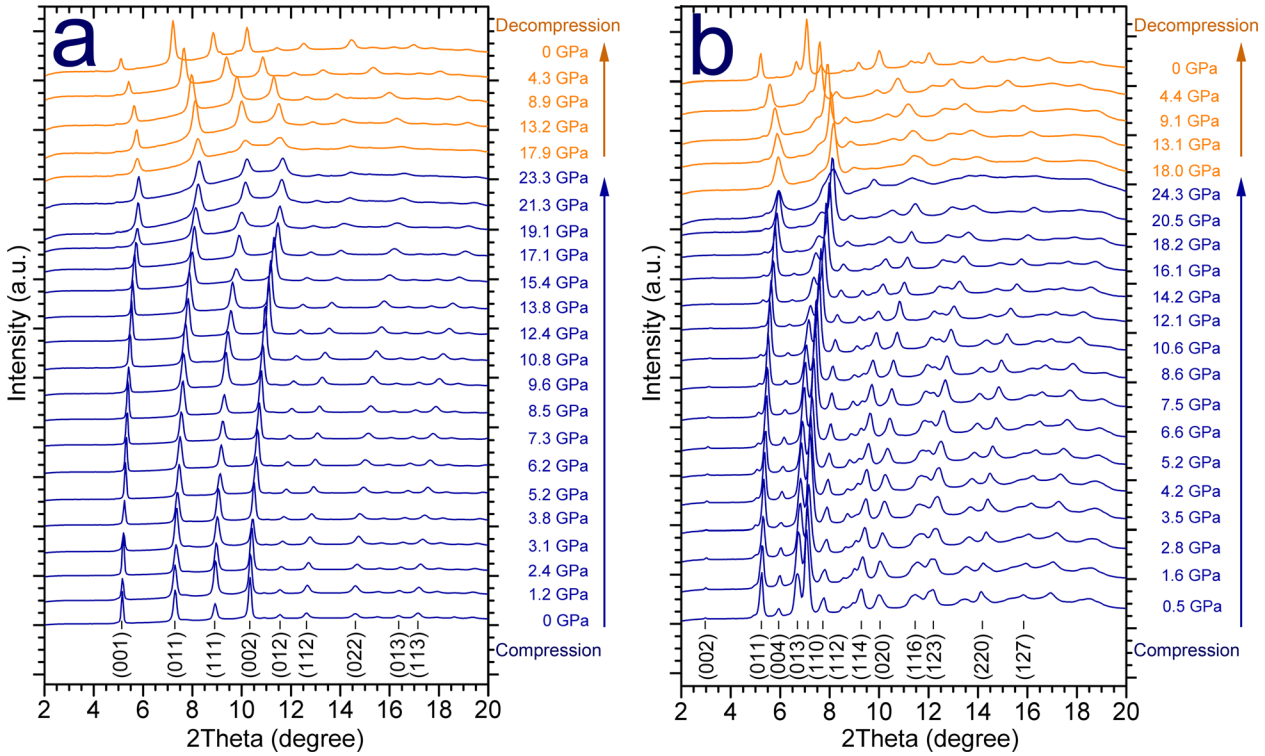

FIG. 2. *In situ* synchrotron XRD pattern of (a) Na_3OBr and (b) Na_4OI_2 upon compression and decompression. No phase transition was observed up to about 24 GPa for both cases. The structures for Na_3OBr and Na_4OI_2 are *Pm*-3*m* and *I*4/*mmm*, respectively.

The cell parameters of both Na_3OBr and Na_4OI_2 were obtained by Rietveld refinements of the XRD data under pressure. Fig. 3 represents the representative refinement plots of Na_3OBr at 1.7 GPa and Na_4OI_2 at 1.6 GPa. The ambient anti-perovskite structures with space groups *Pm*-3*m* and *I*4/*mmm* fit well for Na_3OBr and Na_4OI_2 under pressure, respectively, giving slightly decrescent unit cell parameters. Fig. 4(a) shows the cell parameter evolution of Na_3OBr and Na_4OI_2 as a function of pressure. Nearly linear compression behavior is observed for both lattice parameters *a* of Na_3OBr and *a*/*c* of

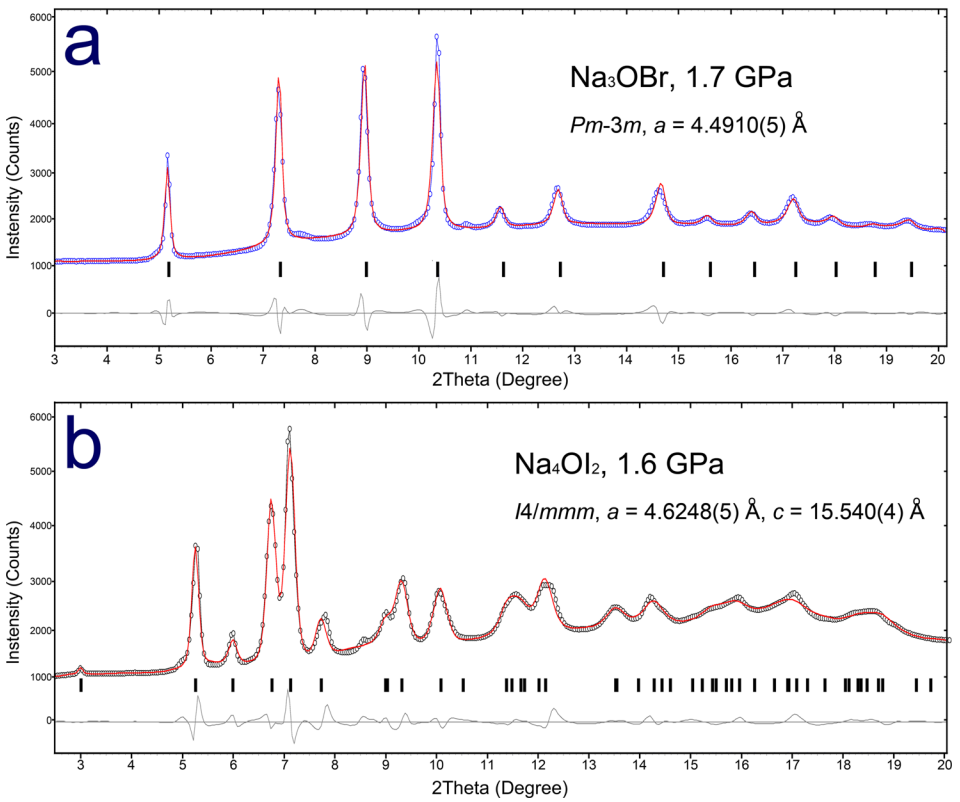

FIG. 3. Rietveld refinement plots of (a) Na_3OBr at 1.7 GPa with space group *Pm*-3*m*, $a = 4.4910(5)$ Å and (b) Na_4OI_2 at 1.6 GPa with space group *I*4/*mmm*, $a = 4.6248(5)$ Å, $c = 15.540(4)$ Å. (Experimental: circle; simulation: red lines; Bragg reflections: black bars; and derives: gray lines.)

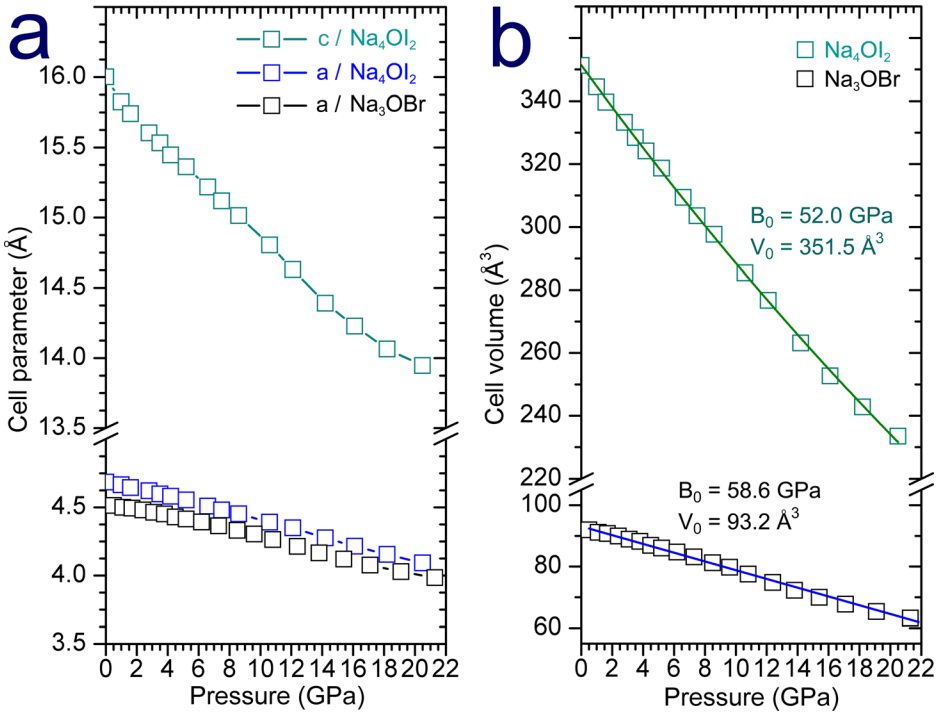

FIG. 4. (a) Cell parameters of Na_3OBr and Na_4OI_2 as a function of pressure. (b) Pressure dependence of the unit cell volume V for cubic Na_3OBr and tetragonal Na_4OI_2. The green and blue lines in (b) represent a fit to the third-order Birch-Murnaghan equation of state.

Na_4OI_2. The compression ratios along the a and c axes of Na_4OI_2 (a/a_0 *vs* c/c_0) remain almost the same with pressure. Fig. 4(b) displays the pressure dependence of the unit cell volume V of Na_3OBr and that of Na_4OI_2 at room temperature, respectively. The green and blue lines are the fit results using the third-order Birch-Murnaghan equation of state[32]

$$P = 3/2B_0[(V/V_0)^{-7/3} - (V/V_0)^{-5/3}] \times \{1 + 3/4(B_0' - 4)[(V/V_0)^{-2/3}] - 1\}.$$

Here, B_0 is the bulk modulus at 0 GPa and B_0' is the derivative of B_0 at 0 GPa, V is the volume at pressure P, and V_0 is the volume at 0 GPa. A least-squares fitting to the measured P-V data in the above-mentioned pressure range yields $B_0 = 58.6$ GPa and $B_0 = 52.0$ GPa for Na_3OBr and Na_4OI_2, respectively, with a fixed B_0' of 4.0. The fit also yields $V_0 = 93.2$ Å^3 for Na_3OBr and $V_0 = 351.5$ Å^3 for Na_4OI_2, which are close to the measured values at ambient pressure. These results suggest that Na-rich antiperovskites are "soft" materials, which may be favorable for hot machining process as solid state electrolytes.

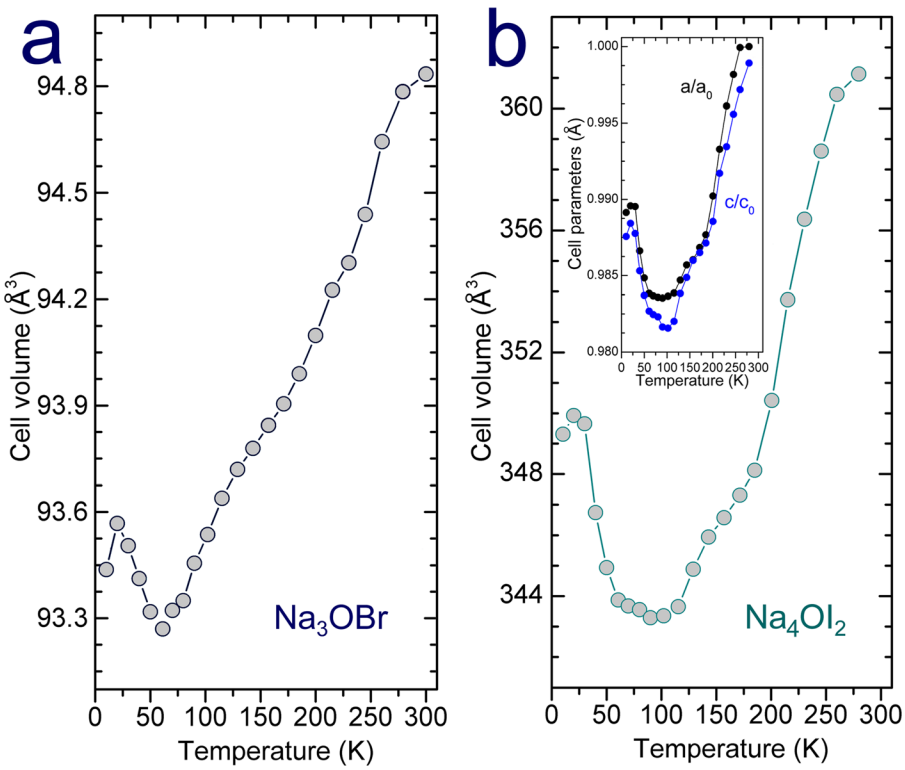

FIG. 5. Temperature dependent cell volume evolution of (a) Na_3OBr and (b) Na_4OI_2 at ambient pressure. The inset of (b) shows the cell parameters of tetragonal Na_4OI_2 as a function of temperature.

B. Negative thermal expansion

Negative thermal expansion has been extensively reported in transition metal based antiperovskites Mn_3AN (A = Zn, Ga, Cu). Dual contributions from the rigid building blocks and magnetic interactions have been suggested as playing key roles in the abnormal structural behavior. However, a nonmagnetic antiperovskite with NTE phenomenon has not been reported yet, which may provide exclusive insight into the underlying mechanism of NTE. Na_3OBr and Na_4OI_2 are suitable candidates for this purpose. Fig. 5 shows the temperature dependent cell volume evolutions for Na_3OBr and Na_4OI_2. During a wide range from room temperature to 100 K, both materials show normal lattice contraction behavior upon cooling. While, at lower temperature ranges (20–55 K for Na_3OBr and 20–80 K for Na_4OI_2, respectively), NTE was observed in both compounds. The observation of NTE in both three-dimensional and intergrowth antiperovskites suggests that NTE could be a universal behavior of materials with antiperovskite structures at low temperature. As they are non-transition-metal systems, the NTE behavior can be only attributed to the lattice effect despite the fact that the distortion mechanism, including octahedron tilting or elongation, has been ruled out by XRD data. We also evaluated the temperature-dependent lattice contraction of the layered Na_4OI_2 along different crystallographic a and c axes. As shown in the inset of Fig. 5(b), both directions exhibit NTE in the 20–80 K range with minimal differences.

C. First-principles calculations

To garner in-depth insights into the pressure- and temperature-dependent structural behaviors of alkali-metal-rich antiperovskites, first-principles calculations were conducted on several Na_3OBr analogues. According to the experimental evidence, Na_3OBr with cubic antiperovskite structure is stable under high pressure without any symmetry change. To evaluate the phase stability of Na_3OBr with distortions, first two artificial crystal structures of Na_3OBr with subgroups of space group Pm-3m, i.e., $P4/mmm$ and R-3m, were generated to simulate typical cell elongation along the four- and three- fold rotation axes. The total energy and cell volumes as a function of pressure are shown in Fig. 6(a). After structure optimization, the two distorted structures present identical energy and cell volume with the cubic

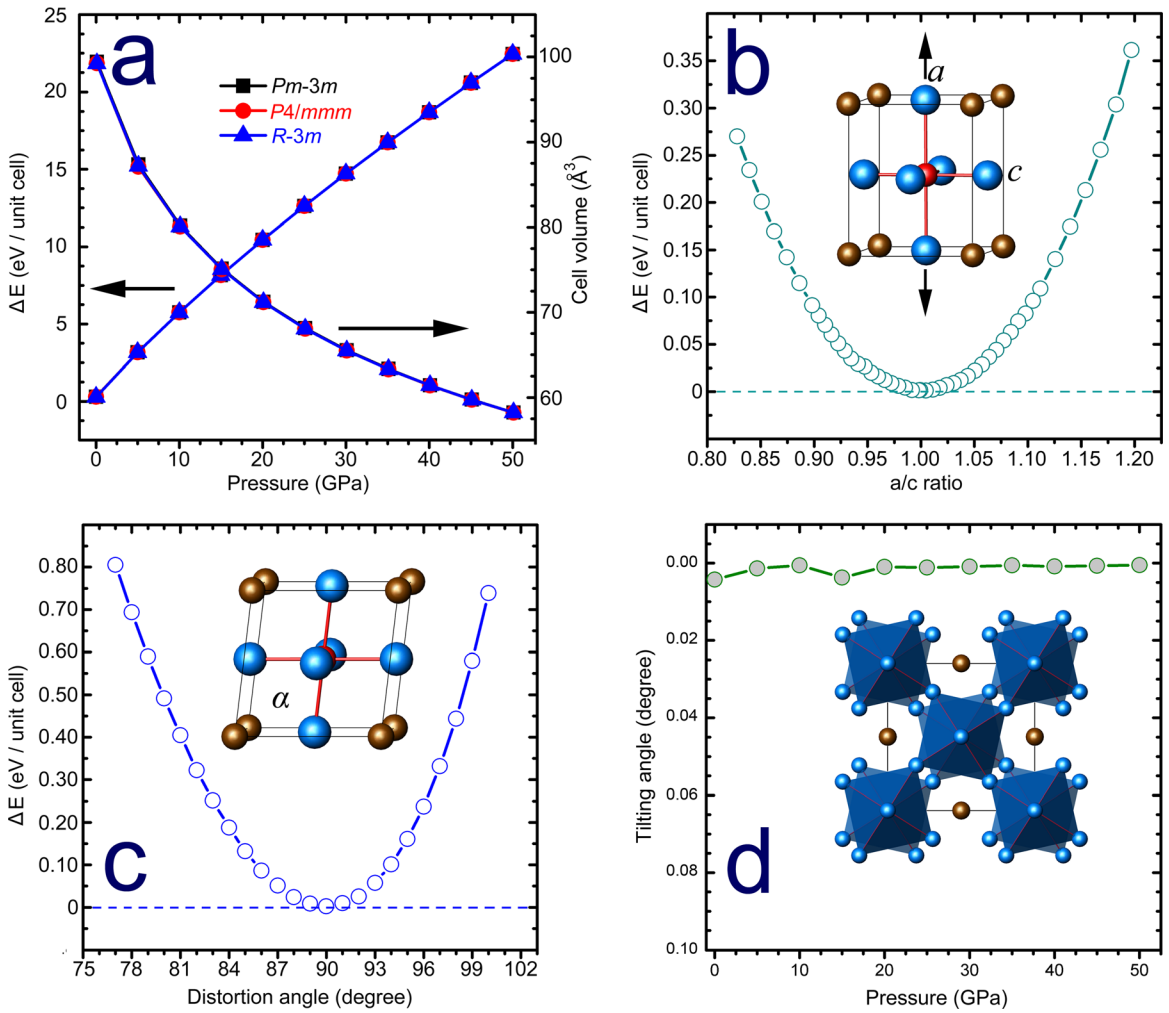

FIG. 6. First-principles calculation results on (a) total energy and cell volume for Na_3OBr with cubic, tetragonal, and trigonal symmetries, and total energy as a function of (b) a/c ratio in the tetragonal structure ($P4/mmm$), (c) distortion angle in the trigonal structure (R-3m) and (d) tilting angle of ONa_6 octahedra in the structure with space group $I4/mcm$. The insets of (b)–(d) show the distortion and rotation manners of the ONa_6 octahedron.

Na_3OBr structure. The extent of distortion of the resulting tetragonal and trigonal structures turns out very small: *a*/*c* ratio is close to 1 and α angle is close to 90°. The results indicate that alkali-metal-rich antiperovskites represented by Na_3OBr prefer the undistorted cubic structure. We also calculated the total energy of the tetragonal and trigonal Na_3OBr structures as a function of *a*/*c* ratio and α angle, respectively, as shown in Figs. 6(b) and 6(c). When ONa_6 deviates from perfect octahedron, the total energies of the structures increase quickly, indicating the instability of Na_3OBr with distorted structures from the original cubic one. Octahedral rotation is another common phenomenon besides distortion that can result in symmetry breaking in perovskite-type structures. The energy landscapes of octahedral rotational modes were used to estimate the stability of Li_3OCl antiperovskite in Chen's recent work.[33] In our experiment, a $\sqrt{2} \times \sqrt{2} \times 2$ supercell with space group *I*4/*mcm* was used to simulate the simplest $a^0a^0c^+$ rotation of ONa_6 in Na_3OBr structure. The rotation angle was relaxed, and the structure was optimized as a function of hydrostatic pressure (as shown in Fig. 6(d)). We can see that there is almost no rotation in the 0–50 GPa range, indicating that such main-group elements dominated antiperovskites prefer cubic structure without rotation. All the above evidences indicate that, although ONa_6 octahedron looks like a nonflexible structural motif, it is not really rigid compared to the transition metal based perovskites.

IV. CONCLUSIONS

In conclusion, we investigated the compressibility and thermal expansion behaviors of antiperovskites Na_3OBr and Na_4OI_2. Both compounds are soft materials with small bulk modulus that make them favorable to be used as electrolytes. The cubic Na_3OBr and intergrowth Na_4OI_2 structures are stable up to 23 GPa. Despite the layered structure feature, Na_4OI_2 shows almost isotropic compressibility along crystallographic *a* and *c* axes. Negative thermal expansion was observed at low temperatures, 20–55 K for Na_3OBr and 20–80 K for Na_4OI_2, in these transition-metal-free antiperovskites for the first time. The phase stability and symmetry preferences among various possible polymorphisms were explained qualitatively on the basis of first-principles calculations. These results provide a more comprehensive understanding of negative thermal expansion in lattice-only antiperovskite systems.

ACKNOWLEDGMENTS

This work was supported by DOE-BES X-ray Scattering Core Program under Grant No. DE-FG02-99ER45775. The UNLV High Pressure Science and Engineering Center (HiPSEC) is a DOE-NNSA Center of Excellence supported by Cooperative Agreement No. DE-NA0001982. HPCAT operations are supported by DOE-NNSA under Award No. DE-NA0001974 and DOE-BES under Award No. DE-FG02-99ER45775, with partial instrumentation funding by NSF. APS was supported by DOE-BES, under Contract No. DE-AC02-06CH11357. Y.W. thanks the help and useful discussion from Professor Z. S. Lin (TIPC, CAS) for computational calculations.

[1]M. A. Peña and J. L. G. Fierro, Chem. Rev. **101**, 1981–2017 (2001).
[2]B. V. Lotsch, Angew. Chem., Int. Ed. **53**, 635–637 (2014).
[3]P. Tong, B.-S. Wang, and Y.-P. Sun, Chin. Phys. B **22**, 067501 (2013).
[4]P. Tong and Y. P. Sun, Adv. Condens. Matter Phys. **2012**, 903239.
[5]K. Takenaka, T. Hamada, D. Kasugai, and N. Sugimoto, J. Appl. Phys. **112**, 083517 (2012).
[6]J. C. Lin, B. S. Wang, S. Lin, P. Tong, W. J. Lu, L. Zhang, W. H. Song, and Y. P. Sun, J. Appl. Phys. **111**, 043905 (2012).
[7]Y. Sun, C. Wang, Y. Wen, L. Chu, H. Pan, and M. Nie, J. Am. Ceram. Soc. **93**, 2178–2181 (2010).
[8]P. Tong, D. Louca, G. King, A. Llobet, J. C. Lin, and Y. P. Sun, Appl. Phys. Lett. **102**, 041908 (2013).
[9]R. Huang, L. Li, F. Cai, X. Xu, and L. Qian, Appl. Phys. Lett. **93**, 081902 (2008).
[10]C. Wang, L. Chu, Q. Yao, Y. Sun, M. Wu, L. Ding, J. Yan, Y. Na, W. Tang, G. Li, Q. Huang, and J. W. Lynn, Phys. Rev. B **85**, 220103 (2012).
[11]Y. Zhao and L. L. Daemen, J. Am. Chem. Soc. **134**, 15042–15047 (2012).
[12]A. Emly, E. Kioupakes, and A. Van der Ven, Chem. Mater. **25**, 4663–4670 (2013).
[13]M. H. Braga, J. A. Ferreira, V. Stockhausen, J. E. Oliveira, and A. El-Azab, J. Mater. Chem. A **2**, 5470–5480 (2014).
[14]Y. Wang, Q. Wang, Z. Liu, Z. Zhou, S. Li, J. Zhu, R. Zou, Y. Wang, J. Lin, and Y. Zhao, J. Power Sources **293**, 735–740 (2015).
[15]J. Chen, L. Hu, J. Deng, and X. Xing, Chem. Soc. Rev. **44**, 3522–3567 (2015).
[16]J. S. O. Evans, J. Chem. Soc., Dalton Trans. **1999**, 3317–3326.
[17]C. Lind, Materials **5**, 1125–1154 (2012).
[18]T. A. Mary, J. S. O. Evans, T. Vogt, and A. W. Sleight, Science **272**, 90–92 (1996).
[19]S. E. Tallentire, F. Child, I. Fall, L. Vella-Zarb, I. R. Evans, M. G. Tucker, D. A. Keen, C. Wilson, and J. S. O. Evans, J. Am. Chem. Soc. **135**, 12849–12856 (2013).
[20]A. Sanson, Chem. Mater. **26**, 3716–3720 (2014).
[21]A. L. Goodwin, M. Calleja, M. J. Conterio, M. T. Dove, J. S. O. Evans, D. A. Keen, L. Peters, and M. G. Tucker, Science **319**, 794–797 (2008).
[22]T. Chatterji, T. C. Hansen, M. Brunelli, and P. F. Henry, Appl. Phys. Lett. **94**, 241902 (2009).
[23]B. K. Greve, K. L. Martin, P. L. Lee, P. J. Chupas, K. W. Chapman, and A. P. Wilkinson, J. Am. Chem. Soc. **132**, 15496–15498 (2010).
[24]K. Takenaka, K. Asano, M. Misawa, and H. Takagi, Appl. Phys. Lett. **92**, 011927 (2008).
[25]T. Hamada and K. Takenaka, J. Appl. Phys. **109**, 07E309 (2011).
[26]K. Takenaka and H. Takagi, Appl. Phys. Lett. **87**, 261902 (2005).
[27]Z. Chen, R. Huang, X. Chu, Z. Wu, Z. Liu, Y. Zhou, and L. Li, Cryogenics **52**, 629–631 (2012).
[28]X. Song, Z. Sun, Q. Huang, M. Rettenmayr, X. Liu, M. Seyring, G. Li, G. Rao, and F. Yin, Adv. Mater. **23**, 4690–4694 (2011).
[29]C. Park, D. Popov, D. Ikuta, C. Lin, C. Kenney-Benson, E. Rod, A. Bommannavar, and G. Shen, Rev. Sci. Instrum. **86**, 072205 (2015).
[30]S. J. Clark, M. D. Segll, C. J. Pickard, P. J. Hasnip, M. I. J. Probert, K. Refson, and M. C. Payne, Z. Kristallogr. **220**, 567–570 (2005).
[31]D. M. Ceperley and B. J. Alder, Phys. Rev. Lett. **45**, 566 (1980).
[32]F. Birch, Phys. Rev. **71**, 809–824 (1947).
[33]M.-H. Chen, A. Emly, and A. Van der Ven, Phys. Rev. B **91**, 214306 (2015).